chemosensors

Article

CRDS Technology-Based Integrated Breath Gas Detection System for Breath Acetone Real-Time Accurate Detection Application

Jing Sun [1], Dongxin Shi [2], Le Wang [3], Xiaolin Yu [4], Binghong Song [5], Wangxin Li [2], Jiankun Zhu [5], Yong Yang [5], Bingqiang Cao [1,*] and Chenyu Jiang [2,*]

[1] School of Materials Science and Engineering, University of Jinan, Jinan 250022, China; sunj@sibet.ac.cn
[2] Suzhou Institute of Biomedical Engineering and Technology, Chinese Academy of Sciences, Suzhou 215163, China; shidx@sibet.ac.cn (D.S.); liwx@sibet.ac.cn (W.L.)
[3] Physical Education Department, Shandong Traditional Chinese Medicine University, Jinan 250355, China; 18253121729@163.com
[4] Jinan Science and Technology Innovation Promotion Center, Jinan 250014, China; yuxiaolin@jn.shandong.cn
[5] Jinan Guoke Medical Technology Development Co., Ltd., Jinan 250001, China; songbh@sibet.ac.cn (B.S.); zhujk@sibet.ac.cn (J.Z.); yangyong@sibet.ac.cn (Y.Y.)
* Correspondence: mse_caobq@ujn.edu.cn (B.C.); jiangcy@sibet.ac.cn (C.J.); Tel.: +86-150-5312-5919 (B.C.); +86-134-0261-7742 (C.J.)

Abstract: The monitoring of acetone in exhaled breath is expected to provide a noninvasive and painless method for dynamic monitoring of summarized physiological metabolic status during obesity treatment. Although the commonly used Mass Spectrometry (MS) technology has high accuracy, the long detection time and large equipment size limit the application of daily bedside detection. As for the real-time and accurate detection of acetone, the gas sensor has become the best choice of gas detection technology, but it is easy to be disturbed by water vapor in breath gas. An integrated breath gas detection system based on cavity ring-down spectroscopy (CRDS) is reported in this paper, which is a laser absorption spectroscopy technique with high-sensitivity detection and absolute quantitative analysis. The system uses a 266 nm single-wavelength ultraviolet laser combined with a breath gas pretreatment unit to effectively remove the influence of water vapor. The ring-down time of this system was 1.068 µs, the detection sensitivity was 1 ppb, and the stability of the system was 0.13%. The detection principle of the integrated breath gas detection system follows Lambert–Beer's law, which is an absolute measurement with very high detection accuracy, and was further validated by Gas Chromatography–Mass Spectrometer (GC-MS) testing. Significant differences in the response of the integrated breath gas detection system to simulated gases containing different concentrations of acetone indicate the potential of the system for the detection of trace amounts of acetone. Meanwhile, the monitoring of acetone during obesity treatment also signifies the feasibility of this system in the dynamic monitoring of physiological indicators, which is not only important for the optimization of the obesity treatment process but also promises to shed further light on the interaction between obesity treatment and physiological metabolism in medicine.

Keywords: obesity treatment; CRDS; breath acetone; breath pretreatment; real-time; accurate detection

check for updates

Citation: Sun, J.; Shi, D.; Wang, L.; Yu, X.; Song, B.; Li, W.; Zhu, J.; Yang, Y.; Cao, B.; Jiang, C. CRDS Technology-Based Integrated Breath Gas Detection System for Breath Acetone Real-Time Accurate Detection Application. *Chemosensors* **2024**, *12*, 261. https://doi.org/10.3390/chemosensors12120261

Received: 11 November 2024
Revised: 10 December 2024
Accepted: 11 December 2024
Published: 13 December 2024

Copyright: © 2024 by the authors. Licensee MDPI, Basel, Switzerland. This article is an open access article distributed under the terms and conditions of the Creative Commons Attribution (CC BY) license (https://creativecommons.org/licenses/by/4.0/).

1. Introduction

Obesity has become a serious problem threatening human health which is a chronic metabolic disease caused by a variety of factors and may cause many kinds of metabolic disorders such as hypertension, diabetes, cardiovascular disease, and so on. A recent study showed that the global population of obese people was upwards of about 1 billion in 2022 [1]. Controlling weight and maintaining a healthy body condition are the main goals of obesity management. Currently, lifestyle interventions, pharmacotherapy, gene therapy, and weight loss surgery are usually used for obesity management and provide targeted

guidance for obese patients and their clinicians in weight management, and the effects are usually evaluated by weight loss [2]. This evaluation method is intuitive and relatively convenient to realize, but it has nuance and limitations for fully and accurately responding to the status of human fat metabolism.

Breath gas detection has been a non-invasive method for disease diagnosis and metabolic status monitoring for the past few years. The changes in the composition and content of trace Volatile Organic Compounds (VOCs) contained in exhaled gas reflect the changes in the internal environment of the human body, which could be applied for the noninvasive detection of many diseases, such as lung cancer, cirrhosis of the liver, breast cancer, and diabetes mellitus [3–8]. Among the VOCs from breath gas, acetone is able to effectively respond to the level of lipolysis and metabolism when the body's glucose supply is insufficient, and it is an important biomarker of human glucose metabolism in respiratory gases. For instance, the amount of acetone produced will increase when the patient's fat metabolism accelerates during obesity treatment. Meanwhile, acetone is highly volatile, and the excess acetone will appear in human exhaled gas at concentrations much higher than the upper level in the range of healthy people (0.5–2.0 ppm) during gas exchange or blood circulation in the human body [9,10]; so, it could provide an important basis for real-time accurate monitoring of human metabolism during obesity treatment. Therefore, accurate real-time detection of acetone content in respiratory gas has become a potential method for monitoring the effectiveness of obesity treatment, which makes up for the inadequacy of the current unitary and limited means of detection.

Gas chromatography (GC), Mass Spectrometry (MS), and electrochemistry (ECM) all can realize the accurate detection of acetone in respiratory gases, but they have drawbacks such as cumbersome sample preconcentration, poor detection selectivity, baseline drift, and time-consuming detection, which lead to these methods not being suitable for real-time and large-scale clinical testing applications [11–16]. On the other hand, laser spectroscopy has the advantages of robustness, short response time, and high detection sensitivity [17–19]. Among the kinds of spectral detection technologies, the cavity ring-down spectroscopy (CRDS) technique has a very high detection sensitivity by increasing the equivalent absorption path through the optical properties of the resonant cavity. However, the sensitivity and stability of CRDS detection is largely influenced by the water vapor content of the ambient gas. Therefore, elucidating how to reduce the water vapor concentration has become the key to accurate detection of respiratory acetone by CRDS technology. Wang et al. [20] successfully eliminated water vapor interference by heating the decay chamber to 40 °C. Hancock [21] et al. achieved water vapor removal by cooling the breathing gas with pretreatment at −20 °C. Jiang et al. [22] used a 0.22 μm filter to deal with the moisture content in the breathing gas. But the methods above are complicated in operation, high in cost, and poor in adsorption performance, and there is an urgent need for a breath acetone detection system based on CRDS technology which is less disturbed by moisture and has high sensitivity and accuracy.

In this study, we designed and constructed an integrated detection system for respiratory acetone with respiratory gas pretreatment based on CRDS technology by utilizing the unique spectral absorption property of the acetone molecule at 266 nm and the water vapor adsorption property of porous activated carbon material. The breath acetone detection accuracy and sensitivity of the designed system were verified through comparative experiments. Further, the breath acetone concentration of obese patients during treatment was tracked and monitored to verify the clinical value of the integrated breath gas detection system in the dynamic monitoring of physiological indexes of obesity. The experiment results showed that the detection system can reduce the interference of water vapor on the accuracy of acetone detection through the breath gas pretreatment unit, the detection accuracy can reach ppb level, and its detection results have good consistency compared with GC-MS. The system has the advantages of high sensitivity, good stability, and fast response speed for real-time clinical testing applications of breath acetone.

2. Materials and Methods

2.1. Basic Principles of CRDS Technology

CRDS is a laser absorption spectroscopy technique with high-sensitivity detection and absolute quantitative analysis, and the basic schematic of CRDS technology is shown in Figure 1.

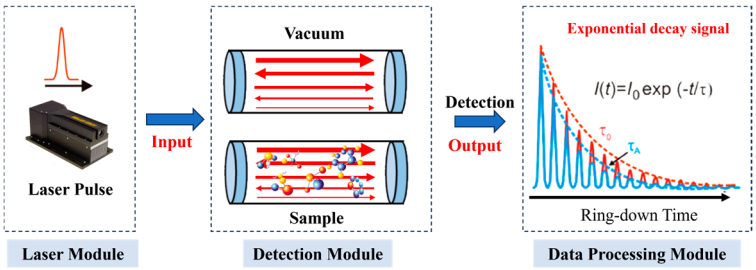

Figure 1. Basic schematic of CRDS technology.

The incident beam is reflected back and forth in a resonant cavity consisting of a highly reflective mirror and a cavity, while the intensity of the beam transmitted after absorption by the sample is detected, according to Lambert–Beer's law [9,23–25]:

$$I(v) = I_0 e^{-\alpha(v)d} \tag{1}$$

where I_0 is the initial intensity of the incident beam, $I(v)$ is the intensity of the outgoing beam, v is the wavelength, e is the natural constant, d is the length of the resonant cavity, and $\alpha(v)$ is the absorption coefficient of the substance to be measured. Therefore, the light intensity in the resonant cavity shows a mono-exponential decay.

It can be calculated from the relationship between $\sigma(v)$ (absorption cross section of the substance to be measured) and $\alpha(v) = n * \sigma(v)$:

$$\tau_0 = \frac{d}{c(1-R)} \tag{2}$$

$$\tau = \frac{d}{c(1-R+\sigma(v)nd)} \tag{3}$$

Therefore, the absorption of the gas sample is as follows:

$$A = \sigma(v)nd = \frac{d}{c}\left(\frac{1}{\tau} - \frac{1}{\tau_0}\right) \tag{4}$$

It follows that the content of the substance to be measured can be obtained by measuring τ_0 and τ.

2.2. Construction of an Integrated Breath Gas Detection System Based on CRDS Technology

The integrated breath gas detection system designed and developed in this paper is based on the basic principle of CRDS mentioned above, and mainly consists of three modules: a laser module, breath acetone detection module, and data processing module, as shown in Figure 2a. Among them, the breath acetone detection module consists of a breath gas pretreatment unit (shown in Figure 2b), a resonance cavity, and a sample injection system. The laser used in the integrated breath gas detection system is an Nd:YAG pumped all-solid-state laser with a center wavelength of 266 nm from Changchun New Industry, which is an electro-optic Q-tuned pulsed laser. The resonant cavity is composed of a cylindrical stainless-steel cavity and a pair of high-reflectance mirrors (Los Gatos Research, U.S.; Purchased in 2016), the length of the stainless-steel cavity is 50 cm, and the cavity is accompanied by three welded standard ports, which are connected to the pressure transducer, vacuum pump, and injection system, respectively. Adjustable flanges are used

in this system to fix the high-reflectance mirrors at both ends of the resonant cavity. The detector is a PMT from Hamamatsu, Japan, which has an integrated high-voltage generator module, and the gain adjustment can be realized by adjusting the control voltage. The data processing module mainly adopts the background deduction algorithm for data processing to obtain the concentration of acetone in the measured sample.

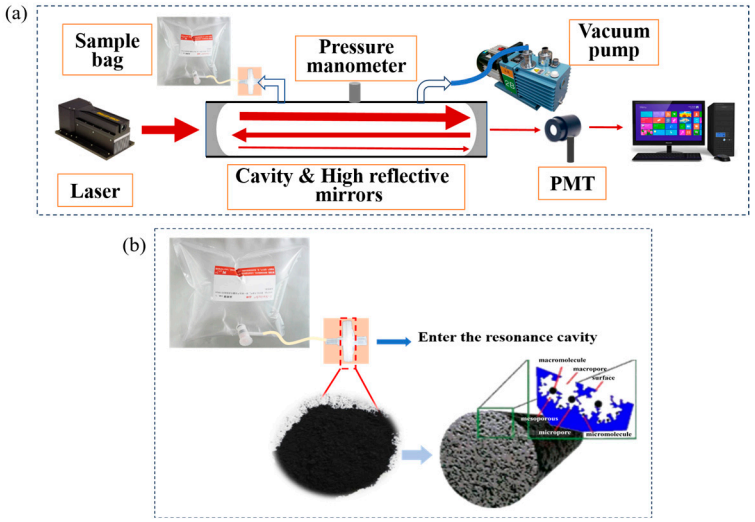

Figure 2. Schematic diagram of (**a**) the structure of the integrated breath gas detection system and (**b**) the breath gas pretreatment unit.

2.3. Preparation of Activated Carbon by Ester Hydrolysis for Breath Gas Pretreatment Unit

First, the graded porous activated carbon material [26,27] prepared in the pre-laboratory stage was soaked in 1 mol/L alkaline solution (KOH) at a ratio of 1:10 for 24 h and then centrifugally washed. Then, the centrifugally washed samples were placed in ethyl acetate solution and stirred and soaked in a stirring heater at 80 °C for 48 h. Finally, the soaked activated carbon was vacuum dried at 100 °C for 24 h to obtain the H-PACs.

The morphologies and microstructures of the samples were examined by scanning electron microscopy (SEM, Quanta 250, FEI, Oxford Instruments, Oxford, UK), transmission electron microscopy (TEM, JEM-2100F, JEOL, Tokyo, Japan), and Fourier Transform Infrared Spectroscopy (FT-IR, iS50, Nicolet Instrument Co., Madison, WI, USA). Samples for FT-IR measurements were obtained over the frequency range of 400–2000 cm^{-1}. Water vapor adsorption experiment data were provided by a micromeritics test.

2.4. Calculation of Acetone Concentration Based on Single-Wavelength Background Deduction Method

According to the basic principle of CRDS, the integrated breath gas detection system designed in this paper adopts the acetone concentration calculation method based on the single-wavelength background deduction method to realize the accurate detection of breath acetone [28,29]. Assuming that the high content of molecules (e.g., N_2, O_2, etc.) in the breath gas is exactly the same in the breath and air as well as the negligible absorption of other VOCs at 266 nm, air is used as the detection background during the specific measurement process, and the decay time constants τ_0, τ_{atm}, and τ_{breath} of vacuum, air, and samples are obtained by alternating the measurements of the vacuum, air, and the sample to be tested, which finally obtains the effective absorption of the air and the sample to be tested:

$$A_{atm} = \sigma(v)nd = \frac{d}{c}\left(\frac{1}{\tau_{atm}} - \frac{1}{\tau_0}\right) \quad (5)$$

$$A_{breath} = \sigma(v)nd = \frac{d}{c}\left(\frac{1}{\tau_{breath}} - \frac{1}{\tau_0}\right) \quad (6)$$

Therefore, the concentration of breath acetone is obtained:

$$\Delta A = A_{breath} - A_{atm} = \sigma(v)nd \quad (7)$$

2.5. Breath Sample Collection Program

A total of 10 obese subjects were recruited for this paper, and breath acetone gas samples were collected every 10 min during obesity treatment. All of the subjects were non-smokers and non-alcoholics and no pregnant or lactating female subjects were recruited. Written informed consent was obtained from all subjects participating in this study, and no cost was subsidized. First, a disposable mouthpiece was attached to the valve of a sampling bag (FEP sampling bag) that had been repeatedly rinsed using high-purity nitrogen. Then, the subject took an appropriate breath, held it in for 3 s, and then exhaled the single breath into the sampling bag. Finally, when the gas volume reached 80% of the sampling bag, the valve of the sampling bag was closed, and the samples were numbered and placed in the holding box.

2.6. Sample Test Methods

Testing of all samples was accomplished on our designed integrated breath gas detection system (shown as Figure 3). First, after the system was warmed up, a baseline test of the system was performed using the ambient gas as a reference. Then, the collected samples were connected to the breath gas pretreatment unit, and after moisture adsorption by activated charcoal, they entered into the resonant cavity for acetone concentration testing, and the sample gases in the resonant cavity were extracted by a vacuum pump after the test was completed. Finally, at the end of each sample test, the resonant cavity is cleaned using high-purity nitrogen gas and repeatedly rinsed at least three times.

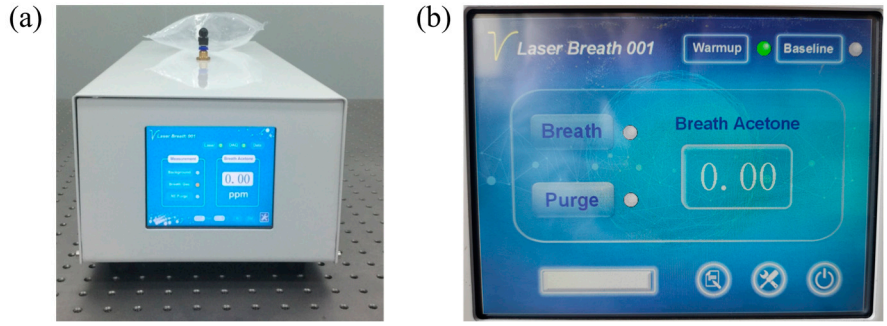

Figure 3. Sample test systems and interfaces: (**a**) Integrated Breath Gas Detection System, and (**b**) Sample test interfaces.

In addition, we tested the breath acetone samples using GC-MS under the following conditions: Analytes absorbed on the SPME fibers were thermally desorbed in a gas chromatography injector at 280 °C. The initial temperature of the column was 5 °C and the column was maintained with carbon dioxide for 3 min. The column is initially heated to 5 °C and maintained with carbon dioxide for 3 min. The temperature was then increased to 250 °C at a rate of 5 °C/min and held for 2 min.

3. Results and Discussion

3.1. Performance of Breath Gas Pretreatment Units

The hydrophilic porous activated carbon material in the breath pretreatment unit is based on the shaped porous activated carbon material prepared in the previous research of our group [26,27], and surface modification was carried out by the ester hydrolysis method to prepare a porous activated carbon material with excellent water vapor adsorption performance (Figure 4). Under alkaline conditions, some oxygen-containing functional groups were formed on the surface of the shaped porous activated carbon by the hydrolysis of ethyl acetate. Its unique pore structure and surface functionalization are more conducive

to the adsorption of water molecules. Breath treated with this material can be free from moisture interference in the test, improving the accuracy of the test.

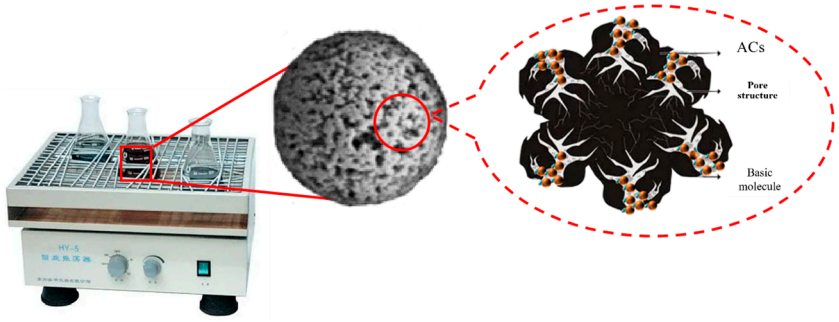

Figure 4. Hydrophilic activated carbon prepared by ester hydrolysis method.

We performed a series of characterizations of the prepared hydrophilic activated carbon materials. Figure 5 shows the SEM and TEM images of H-PACs, respectively. The results showed that the modified activated carbon samples had a good three-dimensional porous structure. Among them, the microporous structure provided more sites for the adsorption of water molecules. From the TEM images, it can be seen that the modified ACs have a unique porous structure as well as a large number of microporous structures, which is conducive to the adsorption of water vapor in the micropores.

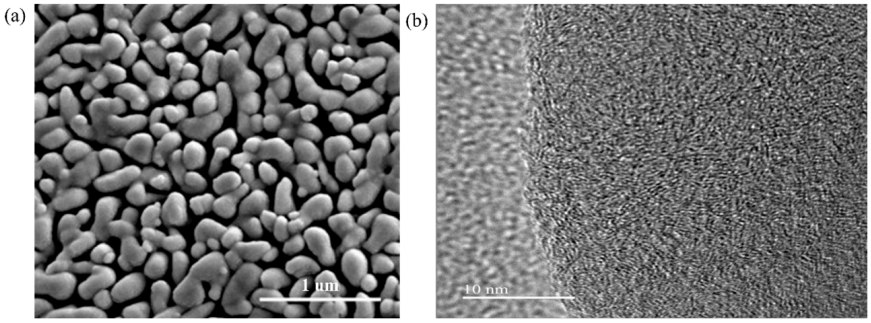

Figure 5. Electron microscope images of H-PACs. (**a**) SEM image; (**b**) TEM image.

Figure 6 compares the N_2 adsorption–desorption isotherms and pore size distribution curves of the H-PACs. According to IUPAC classification, N_2 adsorption isotherms are type I, indicating that they are typical microporous materials [30,31]. As shown in Figure 6a, the type I isotherms of the H-PACs suggest the presence of micropores in the H-PACs, whereas the H4 type hysteresis loops of the H-PACs indicate the presence of both micropores and mesopores. According to the pore size distribution curves of the H-PACs shown in Figure 6b, micropores (0.8 nm~1.5 nm) are dominant in the H-PACs, and there is a unique bimodal pore structure that exists in the H-PACs. Studies have shown that more micropores and smaller mesoporous pores are conducive to water vapor adsorption [32]. Therefore, the H-PACs have the best layered porous structure, which can provide more reaction sites for water vapor adsorption.

Figure 7a shows the FT-IR spectra of the H-PACs. From the figure, it can be seen that the H-PACs prepared by ester hydrolysis modification showed obvious absorption peaks at around 1640, 1410, 1380, and 870 cm^{-1}, which were the vibrational absorption peaks of -C=O and -C-H, respectively [33–35]. This indicates that a large number of functional groups are most likely to be introduced on the surface of H-PACs. Figure 7b shows the adsorption isotherms of the modified sample to water vapor. All of them are V-shaped according to IUPAC classification, which is a typical isotherm for the adsorption of water vapor by activated carbon [36]. From the figure, it can be seen that the adsorption of H-PACs increases with increasing relative pressure at room temperature. This indicates

that the functional groups on the surface of the activated carbon have a greater effect on water vapor adsorption at lower relative pressures, which may be due to the fact that the functional groups act as active centers inducing the movement of water molecules and forming hydrogen bonds with them for water molecule adsorption. Long et al. [37] suggested that the hydrophilic groups bind to water molecules through hydrogen bonding. The adsorption of H-PACs becomes larger as the relative pressure increases. This is mainly due to the fact that water molecules continue to enter into the activated carbon and continue to adsorb at the sites of previously adsorbed water molecules and form water molecule clusters, which break off from each other when they grow to a certain size, thus filling in the micropores [38]. This indicates that the hydrophilic activated carbon prepared by the improved ester hydrolysis method has good water vapor adsorption properties, and it can effectively remove the interference of water in the pretreatment stage of breath to ensure the accuracy of breath acetone detection.

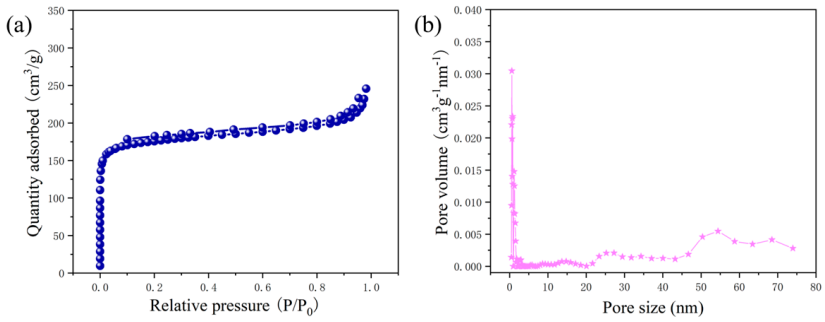

Figure 6. (**a**) N_2 adsorption–desorption isotherms and (**b**) pore size distribution curves of H-PACs.

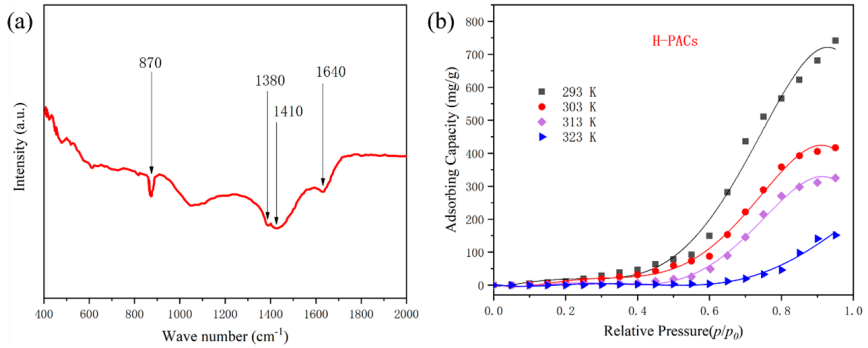

Figure 7. FT-IR (**a**) and isothermal adsorption curve (**b**) of water vapor in H-PACs.

3.2. Performance of the Integrated Breath Gas Detection System

In order to ensure that the absorption of gases within the vacuum decay chamber adheres to the Lambert–Beer law, the ring-down signal under the vacuum of an integrated detection system for breath acetone based on CRDS technology was measured. Figure 8a shows a typical ring-down signal under vacuum acquired by an oscilloscope, with the relative time in the horizontal coordinate and the signal intensity in the vertical coordinate and fitted to the results as shown in Figure 8b. From the figure, it can be seen that the typical ring-down signal shows exponential decay. Further logarithmic operation on the fitted section (0-t) shows that the fitted correlation coefficient is greater than 0.9995, and the fitted residuals and residual sum of squares are 4.25×10^{-4} and 3.16×10^{-4}, respectively, which suggests that the decaying signals obtained by this analytical system are close to the mono-exponential decay conforming to the Lambert–Behr law.

To test the baseline stability of the ring-down time, we continuously measured the vacuum ring-down time constant for 8 h, with each data point being the result of averaging 128 ring-down signals. The typical baseline stability of the system is shown in Figure 9. The results show that the vacuum ring-down time constant t is 1.068 μs with a standard

deviation of 1.35 ns. The stability is defined as the ratio of the standard deviation of the ring-down time constant to the mean over a period of time, i.e., the stability is 0.13%, which is within the satisfied error tolerance.

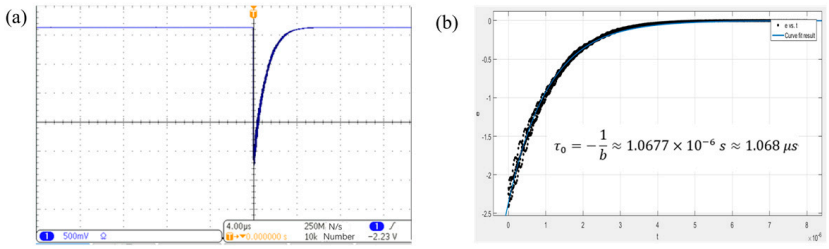

Figure 8. (**a**) Typical ring-down curves; (**b**) single-exponential fitting result curves.

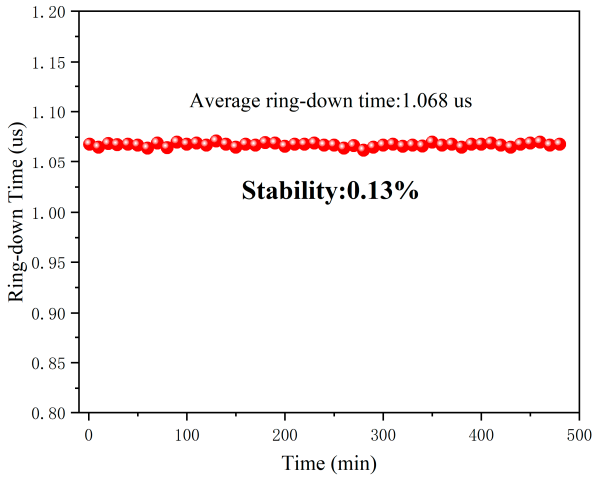

Figure 9. Stability curve of the integrated breath gas detection system.

The accuracy of the measurement by this detection system was further verified by comparing the results with those of GC-MS. The GC-MS test was performed on breath gas samples from healthy individuals in the ion monitoring mode of operation, and the acetone profile obtained is shown in Figure 10a. Figure 10b shows the breath acetone concentrations independently measured using the two methods; the horizontal and vertical coordinates are the acetone concentrations measured using this system and GC-MS, respectively. Based on the test results, the two sets of data were linearly fitted, and the correlation coefficient of the linear fit between the two was R^2 = 0.99924, and the linear relationship was y = 0.9853x + 0.08024, which indicates the consistency of the measurement results of the integrated breath gas detection system based on CRDS technology with the results of GC-MS.

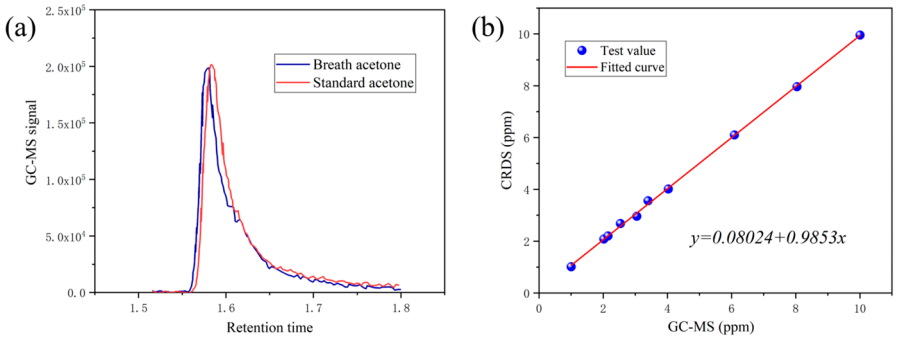

Figure 10. (**a**) GC-MS profiles of breath acetone and (**b**) comparison curve between CRDS-based breath acetone detection system and GC-MS measurement results.

3.3. Application of Integrated Breathing Acetone Detection System

Furthermore, in order to demonstrate the feasibility of this integrated breath gas detection system in the dynamic monitoring of physiological states, the detection system was investigated to monitor the acetone content in the exhaled gas of subjects during obesity treatment (shown as in Figure 11a). Subjects were treated for obesity by massage for 10 min followed by a 5 min rest period, and breath gas samples were collected before, during (10, 15, 25, 30, 40, and 45 min), and in a relaxed state at the end of their massage treatment. The subjects were tested for their response to exhaled gas at different treatment stages, and the corresponding acetone content was calculated based on the ring-down time. As shown in Figure 11b, the acetone content in the breath of the subjects basically remained in a relatively stable state in the calm state before the massage treatment, with its concentration fluctuating between 0.75 and 1.75 ppm, which belongs to the state of the breath acetone level in a normal human body [10].

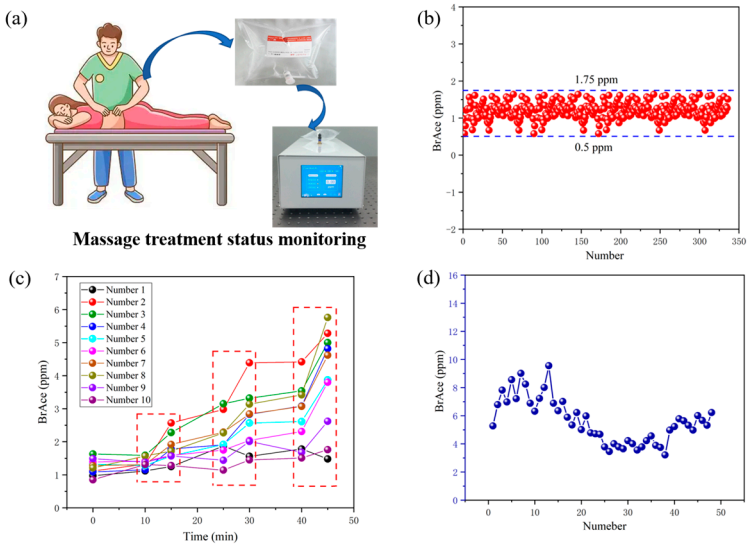

Figure 11. (**a**) Schematic diagram of the response results of the massage treatment process monitoring and detection system. (**b**) The average resting breath acetone concentration profiles for all subjects. (**c**) Curves of changes in breath acetone concentration in subjects during the treatment of obesity with each massage treatment. (**d**) Curves of the breath acetone concentration of subject #2 throughout the course of massage treatment.

The changes in breath acetone during the treatment are shown in Figure 11c. From the figure, it can be seen that after 10 min of massage treatment, the acetone level showed an increasing trend with the increase in massage treatment time, and then, in the relaxed state at the end of the treatment, this gradually declined, which was related to the metabolic process of acetone in the body, and further declined to a level close to that in the resting state before massage. Although subject #1 appeared to have no significant change in breath acetone during a single measurement, his level of breath acetone increased to some degree throughout the course of treatment. During the whole follow-up process of obesity massage therapy, we took subject #2 as an example to analyze the changes in breath acetone concentration during the whole process, and the results were shown in Figure 11d. As can be seen from the figure, subject #2's breath acetone concentration decreased over time as the treatment process progressed, but the lowest concentration at this stage was higher than 4 ppm. In the middle of treatment, the concentration of breath acetone plateaued. As the massage treatment continued, the breath acetone concentration increased again. These results indicate that the developed integrated breath acetone detection system has a promising application in the dynamic real-time monitoring of physiological metabolic states.

4. Conclusions

This study designed and built an integrated detection system for breath acetone detection based on the CRDS technology, which implemented a breath gas pretreatment function by using porous activated carbon material with water vapor adsorption characteristics. This detection system utilized the unique absorption spectrum of acetone molecules at 266 nm and could reduce the interference of water vapor on the accuracy of acetone detection through the breath gas pretreatment unit. The experiment results showed that this novel breath acetone detection system had good consistency compared with GC-MS, so as to realize the accurate detection of breath acetone. Meanwhile, this system had the advantages of high sensitivity, good stability, and a fast response time. Through tracking and monitoring of breath acetone concentration in eight obese patients during the treatment of obesity with a massage method and the changes in body weight indexes, it was proved that the accurate detection of breath acetone by this system could further effectively evaluate the effect of the massage method in the treatment of obesity. The results of the experimental tests showed that the concentration of breath acetone raised with the increase in the treatment time during the treatment of obesity, and the concentration of breath acetone changed significantly after the rest interval of the massage. This may be related to the physiological changes in the body's fat consumption and decomposition as well as the discharging of products from the body after the decomposition. It proved that the integrated breath gas detection system developed in this study had good clinical application prospects for the dynamic real-time monitoring of physiological metabolic states.

Author Contributions: Conceptualization, B.C. and C.J.; methodology, J.S., D.S., X.Y. and L.W.; validation, J.S., D.S., B.S., W.L. and J.Z.; formal analysis, J.Z. and L.W.; investigation, J.Z., W.L. and Y.Y.; resources, B.C. and C.J.; data curation, J.S., D.S., Y.Y. and X.Y.; writing—original draft preparation, J.S. and D.S.; writing—review and editing, B.S. and L.W.; visualization, W.L., B.S. and X.Y.; supervision, J.Z. and Y.Y. All authors have read and agreed to the published version of the manuscript.

Funding: This research received no external funding.

Institutional Review Board Statement: Ethics Committee of the Third Affiliated Hospital of Shandong First Medical University (FY2023037).

Informed Consent Statement: Informed consent was obtained from all subjects involved in this study.

Data Availability Statement: Data are contained within this article.

Acknowledgments: This work is supported by the Taishan Industrial Experts Program (tscx202306125), the Quancheng 5150 Project, and the National Key Research and Development Program (NKRDP): Development of a sterile body fluid culture, monitoring and enrichment system (2022YFC2406204).

Conflicts of Interest: Authors Binghong Song, Jiankun Zhu and Yong Yang were employed by the company Jinan Guoke Medical Technology Development Co., Ltd. The remaining authors declare that the research was conducted in the absence of any commercial or financial relationships that could be construed as a potential conflict of interest.

References

1. Phelps, N.H.; Singleton, R.K.; Zhou, B.; Heap, R.A.; Mishra, A.; Bennett, J.E.; Barbagallo, C.M. Worldwide trends in underweight and obesity from 1990 to 2022: A pooled analysis of 3663 population-representative studies with 222 million children, adolescents, and adults. *Lancet* **2024**, *403*, 1027–1050. [CrossRef] [PubMed]
2. Perdomo, C.M.; Cohen, R.V.; Sumithran, P.; Clément, K.; Frühbeck, G. Contemporary medical, device, and surgical therapies for obesity in adults. *Lancet* **2023**, *401*, 1116–1130. [CrossRef] [PubMed]
3. Romani, A.; Marrone, G.; Celotto, R.; Campo, M.; Vita, C.; Chiaramonte, C.; Carretta, A.; Di Daniele, N.; Noce, A. Utility of SIFT-MS to evaluate volatile organic compounds in nephropathic patients' breath. *Sci. Rep.* **2022**, *12*, 10413. [CrossRef]
4. Tsou, P.-H.; Lin, Z.-L.; Pan, Y.-C.; Yang, H.-C.; Chang, C.-J.; Liang, S.-K.; Wen, Y.-F.; Chang, C.-H.; Chang, L.-Y.; Yu, K.-L.; et al. Exploring Volatile Organic Compounds in Breath for High-Accuracy Prediction of Lung Cancer. *Cancers* **2021**, *13*, 1431. [CrossRef] [PubMed]

5. Sana, S.R.G.L.; Lv, Y.; Chen, G.; Guo, L.; Li, E. Analysis of the volatile organic compounds of epidural analgesia-ameliorated metabolic disorder in pregnant women with gestational diabetes mellitus based on untargeted metabolomics. *Front. Endocrinol.* **2023**, *14*, 1009888. [CrossRef]
6. De Vincentis, A.; Pennazza, G.; Santonico, M.; Vespasiani-Gentilucci, U.; Galati, G.; Gallo, P.; Vernile, C.; Pedone, C.; Antonelli Incalzi, R.; Picardi, A. Breath-print analysis by e-nose for classifying and monitoring chronic liver disease: A proof-of-concept study. *Sci. Rep.* **2016**, *6*, 25337. [CrossRef]
7. Liu, J.; Chen, H.; Li, Y.; Fang, Y.; Guo, Y.; Li, S.; Xu, J.; Jia, Z.; Zou, J.; Liu, G.; et al. A novel non-invasive exhaled breath biopsy for the diagnosis and screening of breast cancer. *J. Hematol. Oncol.* **2023**, *16*, 63. [CrossRef]
8. Nakayama, Y.; Hanada, M.; Koda, H.; Sugimoto, M.; Takada, M.; Toi, M. Reduction of bacterial volatile sulfur compound production by licoricidin and licorisoflavan A from licorice. *J. Breath. Res.* **2022**, *17*, 016006. [CrossRef] [PubMed]
9. Wang, C.; Sahay, P. Breath Analysis Using Laser Spectroscopic Techniques: Breath Biomarkers, Spectral Fingerprints, and Detection Limits. *Sensors* **2009**, *9*, 8230–8262. [CrossRef]
10. Anderson, J.C. Measuring breath acetone for monitoring fat loss: Review. *Obesity* **2015**, *23*, 2327–2334. [CrossRef] [PubMed]
11. Güntner, A.T.; Abegg, S.; Königstein, K.; Gerber, P.A.; Schmidt-Trucksäss, A.; Pratsinis, S.E. Breath Sensors for Health Monitoring. *ACS Sens.* **2019**, *4*, 268–280. [CrossRef]
12. Chapman, E.A.; Baker, J.; Aggarwal, P.; Hughes, D.M.; Nwosu, A.C.; Boyd, M.T.; Mayland, C.R.; Mason, S.; Ellershaw, J.; Probert, C.S.; et al. GC-MS Techniques Investigating Potential Biomarkers of Dying in the Last Weeks with Lung Cancer. *Int. J. Mol. Sci.* **2023**, *24*, 1591. [CrossRef] [PubMed]
13. Du, H.; Sun, R.; Su, J.; Sun, Y.; Xia, K.; Cong, L.; Cui, H. Highly selective acetone detector based on a separation channel and semiconduc-tor gas analyzer. *Meas. Sci. Technol.* **2021**, *32*, 085102. [CrossRef]
14. MG, G.; Bastide, B.H.; Remund, A.L.; Oosthuizen, D.N.; Derron, N.; Gerberb, P.A.; Weber, I.C. Handheld device quantifies breath acetone for real-life metabolic health monitoring. *Anal. Diagn.* **2023**, *2*, 918–928.
15. Zhou, D.; Wang, Q.; Lan, Z.; Chen, Y.; Peng, Z.; Zhang, L.; Liu, Y. Liquid-crystal-based fiber laser ana-lyzer for non-invasive gas detection. *Opt. Lett.* **2023**, *48*, 4508–4511. [CrossRef]
16. Musa-Veloso, K.; Likhodii, S.S.; Cunnane, S.C. Breath acetone is a reliable indicator of ketosis in adults consuming ketogenic meals. *Am. J. Clin. Nutr.* **2002**, *76*, 65–70. [CrossRef] [PubMed]
17. Chen, B.; Li, H.; Zhao, X.; Gao, M.; Cheng, K.; Shao, X.; Wu, H.; Dong, L.; Yin, X. Trace photoacoustic SO_2 gas sensor in SF6 utilizing a 266 nm UV laser and an acousto-optic power stabilizer. *Opt. Express* **2023**, *31*, 6974–6981. [CrossRef] [PubMed]
18. Peng, J.; Cao, Y.; Wang, R.; Wang, G.; Mei, J.; Liu, K.; Chen, W.; Gao, X. Simultaneous Detection of Major Greenhouse Gases with Multiresonator Photoacoustic Spectroscopy. *Anal. Chem.* **2024**, *96*, 14877–14883. [CrossRef]
19. Fu, L.; Zhang, J.; Pan, Y.; Lu, P. Differential photoacoustic spectroscopy for flow gas detection based on single microphone. *Photoacoustics* **2024**, *38*, 2213–5979. [CrossRef]
20. Kentaro, N.; Keisuke, H.; Naoko, N.; Ryuichiro, E.; Mariko, T.; Mai, N.; Hitomi, S.; Misaki, M.; Satoko, T.; Hisako, F.; et al. Ketogenic effects of medium chain triglycerides containing formula and its correlation to breath acetone in healthy volunteers: A randomized, double-blinded, placebo-controlled, single dose-response study. *Front. Nutr.* **2023**, *10*, 1224740.
21. Jiang, C.; Sun, M.; Wang, Z.; Chen, Z.; Zhao, X.; Yuan, Y.; Li, Y.; Wang, C. A portable Real-Time Ringdown Breath Acetone Analyzer: Toward Potential Diabetic Screening and Management. *Sensors* **2016**, *16*, 1199. [CrossRef]
22. Wang, A.; Li, J.; Xu, W.; Yuan, X.; Li, B.; Sun, K.; Liu, J. Air-mediated phosphoric acid activation strategy for preparation of oxygenated functional groups rich activated carbon for capacitive deionization. *Ind. Crops Prod.* **2024**, *215*, 118657. [CrossRef]
23. O'Keefe, A.; Deacon, D.A.G. Cavity ring-down optical spectrometer for absorption measurements using pulsed laser sources. *Rev. Sci. Instrum.* **1988**, *59*, 2544–2551. [CrossRef]
24. Busch, K.W.; Busch, M.A. *Cavity Ringdown Spectroscopy: An Ultra-Trace Absorption Measurement Technique*; ACS Symposium Series; Oxford University Press: New York, NY, USA, 1999; pp. 1–720.
25. Romanini, D.; Lehmann, K.K. Ring-down cavity absorption spectroscopy of the very weak HCN overtone bands with six, seven, and eight stretching quanta. *J. Chem. Phys.* **1993**, *99*, 6287–6301. [CrossRef]
26. Sun, J.; Yang, S.; Ai, J.; Yang, C.; Jia, Q.; Cao, B. Hierarchical Porous Activated Carbon Obtained by a Novel Heating-Rate-Induced Method for Lithium-Ion Capacitor. *Chem. Sel.* **2019**, *4*, 5300. [CrossRef]
27. Sun, J.; Yang, S.H.; Li, S.S.; Cao, B.Q. Double-activated porous carbons for high-performance supercapacitor electrodes. *Rare Met.* **2017**, *36*, 449–456. [CrossRef]
28. Sun, M.; Chen, Z.; Gong, Z.; Zhao, X.; Jiang, C.; Yuan, Y.; Wang, Z.; Li, Y.; Wang, C. Determination of breath acetone in 149 type 2 diabetic patients using a ringdown breath-acetone analyzer. *Anal. Bioanal. Chem.* **2015**, *407*, 1641–1650. [CrossRef] [PubMed]
29. Sun, M.; Zhao, X.; Yin, H.; Wang, Z.; Jiang, C.; Liu, W.; Chen, Z.; Yuan, Y.; Li, Y.; Wang, C. Study of breath acetone and its correlations with blood glucose and blood beta-hydroxybutyrate using an animal model with lab-developed type 1 diabetic rat. *RSC Adv.* **2015**, *5*, 71002–71010. [CrossRef]
30. Cheng, L.S.; Yang, R.T. Improved Horvath-Kawazoe equations including spherical pore models for calculating micropore size distribution. *Chem. Eng. Sci.* **1994**, *49*, 2599–2609. [CrossRef]
31. Finqueneisel, G.; Zimny, T.; Weber, J.V. On the prediction of adsorption isotherms of methanol/water vapour mixtures on microporous activated carbon. *Carbon* **2005**, *43*, 1093–1095. [CrossRef]

32. Samuel, M.S.; Mevada, C.; Mukhopadhyay, M. Hydrophilic Carbon Cloth (Chemically Activated) as an Electrode Material for Energy Storage Device. *Arab. J. Sci. Eng.* **2022**, *47*, 5949–5958. [CrossRef]
33. Tangsathitkulchai, C.; Ngernyen, Y.; Tangsathitkulchai, M. Surface modification and adsorption of eucalyptus wood-based activated carbons: Effects of oxidation treatment, carbon porous structure and activation method. *Korean J. Chem. Eng.* **2009**, *26*, 1341–1352. [CrossRef]
34. Hur, J.; Hwang, B.; Hong, L.; Yoo, S.J.; Chun, S.-E. Fabrication of hydrophilic porous carbon from polyvinylidene chloride-resin via synergetic activation of ZnO and tetrahydrofuran for aqueous supercapacitors. *Surf. Interfaces* **2023**, *40*, 103127. [CrossRef]
35. Canete, S.J.P.; Zhang, Z.Z.; Kong, L.M.; Schlegel, V.L.; Plantz, B.A.; Dowben, P.A.; Lai, R.Y. Application of synchrotron FT-IR microspectroscopy for determination of spatial distribution of methylene blue conjugated onto a SAM via "click" chemistry. *Chem. Commun.* **2011**, *47*, 11918–11920. [CrossRef]
36. Horikawa, T.; Kitakaze, Y.; Sekida, T.; Hayashi, J.; Katoh, M. Characteristics and humidity control capacity of activated carbon from bamboo. *Bioresour. Technol.* **2010**, *101*, 3964–3969. [CrossRef]
37. Long, C.; Li, Y.; Yu, W.H.; Li, A.M. Adsorption characteristics of water vapor on the hypercrosslinked polymeric adsorbent. *Chem. Eng. J.* **2012**, *180*, 106–112. [CrossRef]
38. Brennan, J.K.; Bandosz, T.J.; Thomson, K.T.; Gubbins, K.E. Water in porous carbons. *Colloid. Surf. A* **2001**, *187*, 539–568. [CrossRef]

Disclaimer/Publisher's Note: The statements, opinions and data contained in all publications are solely those of the individual author(s) and contributor(s) and not of MDPI and/or the editor(s). MDPI and/or the editor(s) disclaim responsibility for any injury to people or property resulting from any ideas, methods, instructions or products referred to in the content.